Since January 2020 Elsevier has created a COVID-19 resource centre with free information in English and Mandarin on the novel coronavirus COVID-19. The COVID-19 resource centre is hosted on Elsevier Connect, the company's public news and information website.

Article

Cell Reports

Antibody Treatment of Ebola and Sudan Virus Infection via a Uniquely Exposed Epitope within the Glycoprotein Receptor-Binding Site

Graphical Abstract

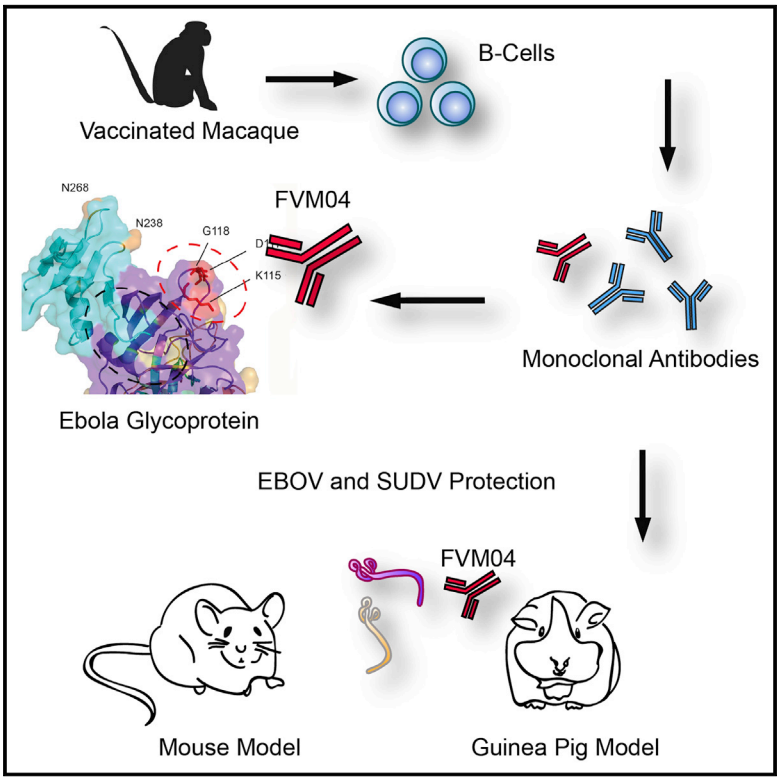

Highlights

- Monoclonal antibody FVM04 blocks interaction of ebolavirus with its host receptor
- FVM04 cross-neutralizes and protects against EBOV and SUDV in rodents
- A new ZMapp version that includes FVM04 protects guinea pigs from EBOV and SUDV
- Specific GP mutations expose epitopes for FVM04 and other cross-neutralizing mAbs

Authors

Katie A. Howell, Xiangguo Qiu, Jennifer M. Brannan, ..., Gary P. Kobinger, John M. Dye, M. Javad Aman

Correspondence

javad@integratedbiotherapeutics.com

In Brief

Howell et al. examine a mAb, FVM04, that binds the ebolavirus receptor-binding site and find that FVM04 protects against EBOV and SUDV. When combined with two ZMapp™ components, the antibody cocktail retains EBOV protection similar to that of ZMapp™ and extends protection against SUDV. Specific glycoprotein mutations that enhance the exposure of cross-neutralizing epitopes are described.

Howell et al., 2016, Cell Reports *15*, 1514–1526
May 17, 2016
http://dx.doi.org/10.1016/j.celrep.2016.04.026

CellPress

OPEN ACCESS
CellPress

Cell Reports
Article

Antibody Treatment of Ebola and Sudan Virus Infection via a Uniquely Exposed Epitope within the Glycoprotein Receptor-Binding Site

Katie A. Howell,[1] Xiangguo Qiu,[2,3,4] Jennifer M. Brannan,[5] Christopher Bryan,[6] Edgar Davidson,[6] Frederick W. Holtsberg,[1] Anna Z. Wec,[10] Sergey Shulenin,[1] Julia E. Biggins,[1] Robin Douglas,[1] Sven G. Enterlein,[1] Hannah L. Turner,[7] Jesper Pallesen,[7] Charles D. Murin,[7,8] Shihua He,[2,3,4] Andrea Kroeker,[2,3,4] Hong Vu,[1] Andrew S. Herbert,[5] Marnie L. Fusco,[8] Elisabeth K. Nyakatura,[11] Jonathan R. Lai,[11] Zhen-Yong Keck,[12] Steven K.H. Foung,[12] Erica Ollmann Saphire,[8,9] Larry Zeitlin,[13] Andrew B. Ward,[7] Kartik Chandran,[10] Benjamin J. Doranz,[6] Gary P. Kobinger,[2,3,4] John M. Dye,[5] and M. Javad Aman[1,*]

[1]Integrated BioTherapeutics, Inc., Gaithersburg, MD 20878, USA
[2]Special Pathogens Program, National Microbiology Laboratory, Public Health Agency of Canada, Winnipeg, MB R3E 3R2, Canada
[3]Deparment of Medical Microbiology
[4]Department of Immunology
University of Manitoba, Winnipeg, MB R3E 0J9, Canada
[5]U.S. Army Medical Research Institute of Infectious Diseases, Frederick, MD 21702, USA
[6]Integral Molecular, Philadelphia, PA 19104, USA
[7]Department of Integrative Structural and Computational Biology
[8]Department of Immunology and Microbial Science
[9]Skaggs Institute for Chemical Biology
The Scripps Research Institute, La Jolla, CA 92037, USA
[10]Department of Microbiology and Immunology
[11]Department of Biochemistry
Albert Einstein College of Medicine, Bronx, NY 10461, USA
[12]Department of Pathology, School of Medicine, Stanford University, Stanford, CA 94305, USA
[13]Mapp Biopharmaceutical, San Diego, CA 92121, USA
*Correspondence: javad@integratedbiotherapeutics.com
http://dx.doi.org/10.1016/j.celrep.2016.04.026

SUMMARY

Previous efforts to identify cross-neutralizing antibodies to the receptor-binding site (RBS) of ebolavirus glycoproteins have been unsuccessful, largely because the RBS is occluded on the viral surface. We report a monoclonal antibody (FVM04) that targets a uniquely exposed epitope within the RBS; cross-neutralizes Ebola (EBOV), Sudan (SUDV), and, to a lesser extent, Bundibugyo viruses; and shows protection against EBOV and SUDV in mice and guinea pigs. The antibody cocktail ZMapp™ is remarkably effective against EBOV (Zaire) but does not cross-neutralize other ebolaviruses. By replacing one of the ZMapp™ components with FVM04, we retained the anti-EBOV efficacy while extending the breadth of protection to SUDV, thereby generating a cross-protective antibody cocktail. In addition, we report several mutations at the base of the ebolavirus glycoprotein that enhance the binding of FVM04 and other cross-reactive antibodies. These findings have important implications for pan-ebolavirus vaccine development and defining broadly protective antibody cocktails.

INTRODUCTION

Filoviruses are the causative agents of severe hemorrhagic fever in humans and nonhuman primates (NHPs) (Kuhn et al., 2014). Members of the family *Filoviridae* include two marburgviruses: Marburg virus (MARV) and Ravn virus (RAVV), and five ebolaviruses: Ebola virus (EBOV), Sudan virus (SUDV), Bundibugyo virus (BDBV), Reston virus (RESTV), and Taï Forest virus (TAFV) (Kuhn et al., 2014). The EBOV (Zaire) has caused the largest number of outbreaks, including the 2014 EBOV disease (EVD) epidemic that led to over 28,637 cases and 11,315 deaths. Due to the higher frequency of outbreaks caused by EBOV, most efforts toward vaccine and therapeutic development have focused on this agent. Several studies have shown remarkable efficacy of antibody therapeutics against EBOV (Dye et al., 2012; Marzi et al., 2012; Olinger et al., 2012; Pettitt et al., 2013; Qiu et al., 2012a, 2012b, 2013a, 2014). However, until recently (Bounds et al., 2015; Flyak et al., 2016; Frei et al., 2016; Holtsberg et al., 2015; Keck et al., 2015), the development of cross-protective monoclonal antibodies (mAbs) targeting multiple species of ebolavirus has been lagging behind.

The filovirus surface glycoprotein, comprising disulfide-linked subunits GP1 and GP2, is the primary target for vaccines and immunotherapeutics (Marzi and Feldmann, 2014). The crystal structures of the trimeric EBOV $GP_{1,2}$ spike (henceforth termed GP) in complex with KZ52 (Lee et al., 2008), a neutralizing mAb

derived from an EVD human survivor (Maruyama et al., 1999), as well as SUDV GP in complex with the neutralizing mouse mAb 16F6 (Dias et al., 2011), have revealed a key mechanism of neutralization. The three GP1 subunits form a chalice-like structure, with GP2 wrapping around GP1 and the N terminus of GP1 forming the base of the chalice (Lee et al., 2008). Both KZ52 and 16F6 contact residues within GP1 and GP2 at the base and neutralize the virus by blocking the viral fusion with the endosomal membrane (Dias et al., 2011; Lee et al., 2008). When administered prophylactically or 1 hr after infection, KZ52 protected guinea pigs from lethal EBOV challenge (Parren et al., 2002). However, in a single study, KZ52 did not protect against EBOV in NHPs at the tested dosing and regimen (Oswald et al., 2007).

Several recent studies have revealed that effective post-exposure protection against EBOV in primates requires a cocktail of mAbs (Pettitt et al., 2013; Qiu et al., 2012a, 2013a) or a combination of mAbs and interferon alpha (IFNα) (Qiu et al., 2013b, 2013c). Further testing of various combinations in the guinea pig model of EBOV infection identified a highly effective cocktail of three EBOV-specific mAbs, known as ZMapp^{TM} (Qiu et al., 2014). ZMapp^{TM} showed 100% efficacy in NHPs when treatment was initiated as late as 5 days post-infection (dpi) (Qiu et al., 2014). Single-particle electron microscopy (EM) reconstructions of GP complexed with individual ZMapp*TM* components (c2G4, c4G7, and c13C6) revealed two sites of vulnerability on the EBOV GP and elucidated the structural basis for their remarkable efficacy (Murin et al., 2014). Of the three components of ZMapp^{TM}, c2G4 and c4G7 target an epitope shared with KZ52 at the "base" of the chalice near the interface of GP1 and GP2, whereas c13C6 binds to a highly glycosylated domain on the top of a GP molecule known as the glycan cap (Davidson et al., 2015; Murin et al., 2014).

While the combination of the base and glycan cap binders thus far appeared to be most effective against EBOV, these antibodies are virus specific, and it is not clear if the same paradigm can be applied to broadly protective immunotherapeutics. Although the epitopes engaged by EBOV-specific KZ52 and SUDV-specific 16F6 overlap by ten residues (Dias et al., 2011; Lee et al., 2008), these base binders do not cross-react with other ebolaviruses. Neutralizing antibodies targeting the receptor-binding site (RBS) have been described for several viruses, including influenza (Lee and Wilson, 2015), HIV (Georgiev et al., 2013), SARS (severe acute respiratory syndrome) coronaviruses (Coughlin and Prabhakar, 2012), and Chikungunya virus (van Duijl-Richter et al., 2015). However, no neutralizing antibodies have been identified that would target the RBS within the ebolavirus glycoproteins. The filovirus RBS consists of a relatively exposed hydrophilic "crest" and a hydrophobic "trough" that is exposed on marburgvirus but occluded by the glycan cap in EBOV GP (Hashiguchi et al., 2015; Wang et al., 2016). RBS-binding mAbs were recently identified for marburgvirus (Flyak et al., 2015) and shown to bind to the RBS trough (Hashiguchi et al., 2015). Some of these antibodies also bind to EBOV GP but only after the glycan cap is proteolytically removed by thermolysin (Hashiguchi et al., 2015), a process that mimics the cathepsin-mediated cleavage in endosomes (Miller and Chandran, 2012). In contrast, no antibodies have been reported to date that bind the prominent crest region of the RBS.

Recently, we reported that pan-ebolavirus and pan-filovirus antibodies, including two broadly neutralizing mAbs isolated from mice and macaques that were immunized with a mixture of engineered glycoproteins for EBOV, SUDV, and MARV and boosted with virus-like particles (VLPs) for the three viruses (Holtsberg et al., 2015; Keck et al., 2015). In contrast to the base binders, these antibodies all bind, to the apex of the GP trimer, either the inner chalice or the glycan cap. Here, we report that one of these mAbs, FVM04, binds to the tip of the RBS crest and blocks the interaction of EBOV GP with its endosomal receptor Niemann-Pick C1 (NPC-1). EM reconstructions of FVM04 complexed with EBOV GP show a unique asymmetric mode of engagement with a single antibody per trimer. FVM04 neutralizes EBOV, SUDV, and, to a lesser extent, BDBV and protects mice and guinea pigs from lethal challenge with EBOV and SUDV. Furthermore, replacement of one of the base binders in ZMapp^{TM} with FVM04 retains the potency of the cocktail toward EBOV while expanding the protective breadth of the cocktail to include SUDV.

RESULTS

FVM04 Binds to an Exposed Region of the Filovirus RBS

We recently described several macaque-derived pan-ebolavirus mAbs (Keck et al., 2015). One of these mAbs (FVM04) neutralized both EBOV and SUDV and showed significant efficacy in mice when administered at two doses, one on the day of challenge and one 3 dpi (Keck et al., 2015). Our studies suggested that FVM04 targets a conformational epitope shared among all ebolaviruses with a low level of cross-reactivity to MARV (Keck et al., 2015). In order to define the FVM04 epitope, we used an alanine scanning approach, where FVM04 binding was evaluated against a "shotgun mutagenesis" mutation library of EBOV GP with 641 of 644 target residues individually mutated. Human HEK293T cells were transfected with the entire library in a 384-well array format (one clone per well; Figure 1A) and assessed for reactivity to FVM04 by high-throughput flow cytometry.

The epitope mapping identified EBOV GP residues K115, D117, and G118 as critical for FVM04 binding (Figure 1). Alanine substitutions at these residues reduced FVM04 binding to 29%, 1%, and 2% of wild-type, respectively, suggesting that these residues constitute key contact sites for FVM04, with D117 and G118 having the greatest energetic contribution to FVM04 binding (Figures 1B and 1C). In contrast, binding of two other pan-ebolavirus antibodies FVM02 and FVM09 (Keck et al., 2015) was not affected by these mutations (Figure 1C). The putative epitope of FVM04 is positioned in a previously described region with a crest-and-trough morphology (Bornholdt et al., 2016; Hashiguchi et al., 2015) within the RBS and constitutes the tip of the hydrophilic crest (red dotted outline in Figure 1D), which interacts with a loop from the endosomal filovirus receptor NPC1 (Wang et al., 2016). In contrast to this exposed tip of the crest, the trough is lined with hydrophobic residues and occluded by the β14-β15 loop within the glycan cap (black dotted outline in Figure 1D). This occlusion explains why trough-binding mAbs do not bind and neutralize EBOV unless the glycan cap is removed by proteolysis (Hashiguchi et al., 2015). Interestingly, while FVM04 binds well to EBOV GP, this binding was moderately enhanced by alanine

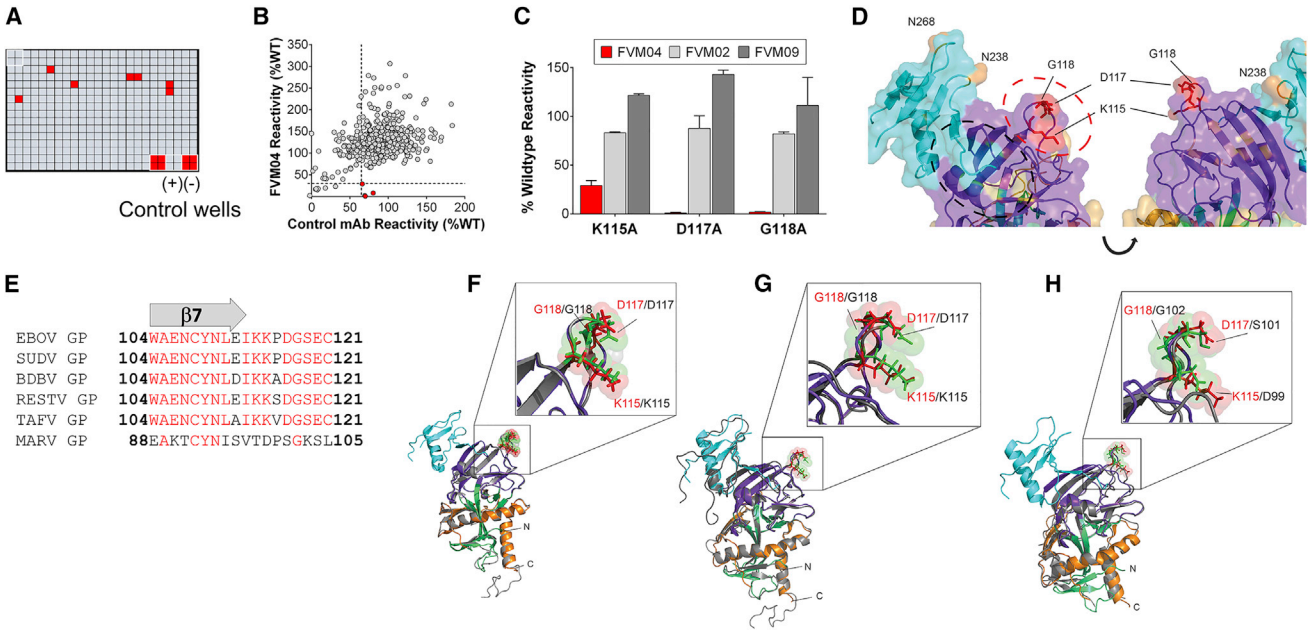

Figure 1. Identification of Critical Residues for FVM04 Binding

(A) A shotgun mutagenesis mutation library was constructed for EBOV GP protein, where each of the 641 amino acids were individually mutated to alanine. Human HEK293T cells expressing the mutation library were tested for reactivity to mAbs using an Intellicyt flow cytometer. A typical reactivity pattern (red wells) is shown for a representative assay plate. Eight positive (wild-type EBOV GP) and eight negative (mock-transfected) control wells were included on each plate.

(B) The library was tested for reactivity with FVM04. Clones with <30% binding relative to that of wild-type (WT) EBOV GP yet >65% reactivity for a control mAb were initially identified to be critical for FVM04 binding.

(C) Mutation of three individual residues reduced FVM04 binding (red bars) but had little effect on the binding of FVM02 and FVM09 (gray bars; Keck et al., 2015). Bars represent the mean and range ([max−min]/2) of at least two replicate data points.

(D) The FVM04 binding residues are shown in red in the crystal structure of EBOV GP. The glycan cap is shown in cyan, and the attachment points for N-linked glycans in orange. The GP1 core is shown in purple, and parts of GP2 are seen in yellow. The RBS crest is shown in red outline and the occluded trough region is shown in black outline.

(E) Sequence homology between filoviruses within the RBS crest region containing putative FVM04 epitope. Identical sequences among ebolavirus species and between ebolavirus and marburgvirus are shown in red. The FVM04 binding site is boxed.

(F–H) The EBOV GP monomer is depicted as a cartoon overlay with GP_{CL} (F), SUDV GP (G), and MARV RAVN GP (H). Putative critical EBOV contacts made by FVM04 are shown as sticks (red) overlaid with corresponding contact residues from the overlay structure (green).

substitution of N238, T240, N257, T259, N268, and T270, mutations that delete three out of four glycosylation sites on the glycan cap (Figure S1), suggesting that these glycans may modestly interfere with FVM04 binding. Nonetheless, these data show that FVM04 represents a prototypic pan-ebolavirus antibody that recognizes a uniquely exposed epitope within the RBS.

The crest region is highly conserved among all ebolavirus species, and the three residues critical for FVM04 binding are 100% identical among ebolaviruses (Figure 1E). An overlay of the crystal structures of EBOV GP (Lee et al., 2008) with the structure of thermolysin-cleaved GP (GP_{CL}) (Bornholdt et al., 2016; Wang et al., 2016) and SUDV GP (Dias et al., 2011) showed high structural conservation within this region and prominent exposure of these residues on the surface of GP_{CL} (Figure 1F) and SUDV GP (Figure 1G). While only one out of the three residues in this putative epitope match between EBOV and MARV (Hashiguchi et al., 2015) (Figure 1E), this region still shows a high degree of conformational similarity between EBOV and MARV, with the three critical EBOV residues overlaying well with MARV D99, S101, and G102 (Figure 1H). This may explain the low affinity of FVM04 for MARV GP as we previously reported (Keck et al., 2015).

EBOV-neutralizing antibodies KZ52 (Lee et al., 2008; Parren et al., 2002), 2G4, and 4G7 (Murin et al., 2014; Qiu et al., 2012b) bind to overlapping epitopes at the base of the GP trimer consisting of residues from both GP2 and the base of GP1 (Figure 2A). In contrast, FVM04 appears to bind the apex of the trimer, between the glycan cap and the trimer center (Figure 2A), therefore representing a distinct class of neutralizing antibodies. In addition to epitope-mapping information (loss-of-function analysis), the alanine-scanning experiments revealed a striking difference between the GP-binding patterns of these "base-binding" and "apex-binding" classes of neutralizers. While the binding of the base binder KZ52 to all individual mutants remained consistently below 150% of wild-type GP (Figure 2B), several single-alanine mutations of GP had a dramatic enhancing effect (as high as 200%–300%) on FVM04 binding (Figure 2C). Out of 217 amino acids forming the base, alanine mutation of 23 residues increased FVM04 binding to GP by more than 2-fold (Figure 2C; Table S1). Most of these residues are hydrophobic, highly networked, and not surface exposed (Figure S2; Table S1). In addition to the 23 base residues, mutation of R498 and R501, within the furin cleavage site separating GP1 and GP2 (Volchkov et al., 1998), also led

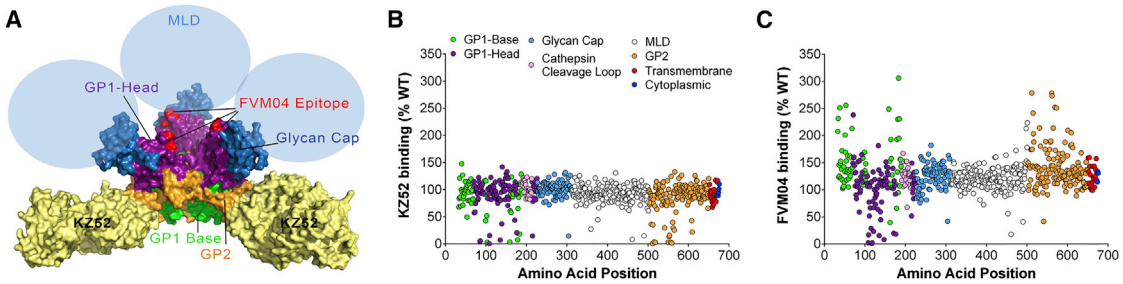

Figure 2. Mutations in the GP Base Affect the Exposure of the FVM04 Epitope

(A) Crystal structure of the trimeric EBOV GP complexed with KZ52 (PDB: 3CSY). The specific domains are color coded as indicated in the figure.

(B and C) Relative binding of individual point mutants of mature EBOV GP to the base binder KZ52 (B) or FVM04 (C) compared to binding to wild-type (WT) GP set at 100%. Individual mutants are color coded in (B) and (C) based on the positioning of each residue in various structural domains according to the key shown in (B). See also Table S1 and Figures S1 and S2.

to an increase over 2-fold in FVM04 binding (Figure 2C; Table S1). An alanine mutagenesis scan of several other cross-reactive apex-binding antibodies (m8C4, 4B8, FVM09, FVM17, and FVM20) (Holtsberg et al., 2015; Keck et al., 2015) also revealed a similar enhancement of binding to the same alanine mutants that enhance FVM04 binding (Table S1). These data suggest that specific mutations in the GP base may have a global impact on the exposure of cross-reactive epitopes in the GP1 head domain. This finding may have major implications for the design of pan-ebolavirus vaccines.

EM Analysis of FVM04-GP Complex

To further characterize FVM04 binding to EBOV GP, FVM04 Fab in complex with GPΔMuc was analyzed by negative-stain EM. The binding location of FVM04 revealed an epitope consistent with the crest residues derived by mutagenesis studies. The class averages suggest that only one FVM04 Fab binds to each GP trimer (Figures 3A and 3B; Figure S3). The binding of one FVM04 Fab per trimer was also further confirmed by size exclusion chromatography-multiangle light scattering (SEC-MALS) analysis (Figure S4). It is likely that the binding orientation and proximity to the 3-fold axis precludes additional FVM04 Fabs from binding. In contrast, the previously characterized glycan-cap-binding antibody c13C6, which binds in a nearby region to FVM04, has a greater occupancy (two to three Fabs per GP trimer) (Murin et al., 2014) (Figure 3C). Although several attempts were made to generate a 3D reconstruction of FVM04 binding to GP, the data failed to converge on an interpretable model, suggesting that the crest epitope is flexible.

Cross-neutralizing Activity of FVM04

We used several assays to evaluate the cross-neutralizing activity of FVM04 against multiple ebolaviruses. These assays included replication-incompetent vesicular stomatitis viruses (VSVs) pseudotyped with filovirus GP and expressing Luciferase (VSV-GP-Luc), as well as replication-competent VSV pseudotypes expressing GFP (VSV-GP-GFP) and wild-type live virus. While the first assay identifies only direct-entry inhibitors, antibodies inhibiting either the entry or other stages of viral replication can be identified by the second assay or live virus. As shown in Figure 4A, FVM04 effectively neutralized the entry of both VSV-pseudotyped EBOV and SUDV, with half maximal effective concentration (EC_{50}) values of 3.4 and 4.3 μg/ml, respectively. We also examined whether the FVM04 neutralization is dependent on bivalent binding of full immunoglobulin (Ig) G or whether FVM04 Fab fragment would also mediate neutralization. EBOV entry was effectively inhibited by FVM04 Fab with an EC_{50} similar to that of full IgG; however, the neutralizing potency of FVM04 Fab toward SUDV was reduced compared to that of full IgG (Figure 4B). FVM04 also effectively neutralized replication-competent VSV pseudotyped with EBOV or SUDV but not TAFV (Figure 4C). While FVM04 showed low neutralizing activity toward VSV-BDBV GP-GFP, this neutralization plateaued at 50%, leaving a non-neutralized subset of infectious virions remaining (Figure 4C). We further tested the neutralizing activity of FVM04 against authentic (wild-type) EBOV, SUDV, and BDBV, using a plaque reduction neutralization (PRNT) assay under BioSafety Level 4 (BSL-4) containment. The highest neutralizing activity was observed against SUDV, while 3- to 4-fold and 20- to 30-fold higher concentrations of FVM04 were required to effectively neutralize wild-type EBOV and BDBV, respectively (Figure 4D). As expected, FVM04 did not neutralize MARV (Figure 4D).

Previous reports showed that mAbs targeting the trough region of the RBS do not or poorly neutralize VSV-EBOV GP but can neutralize the pseudotyped virus after cleavage with thermolysin (VSV-EBOV GP_{CL}), which mimics the cathepsin cleavage in endosomes (Bornholdt et al., 2016; Flyak et al., 2015; Hashiguchi et al., 2015). To this end, we tested whether the crest binder FVM04 could also neutralize the endosomal form of the virus and whether proteolytic removal of the glycan cap and mucin-like domain (MLD) impacts its neutralizing potency. As shown in Figure 4E, FVM04 neutralized both VSV-EBOV GP_{CL} and VSV-SUDV GP_{CL} nearly 100-fold more effectively than the VSV expressing full-length GP (compare with Figure 4C), suggesting that cathepsin cleavage may further expose the FVM04-binding site. Conversely, no increase in the partial neutralization of BDBV by FVM04 was observed upon thermolysin cleavage (Figure 4E).

Inhibition of NPC1 Binding

Given the location of the FVM04 epitope and the antibody's dramatically increased neutralizing efficacy upon thermolysin cleavage, we hypothesized that FVM04 blocks binding of cleaved

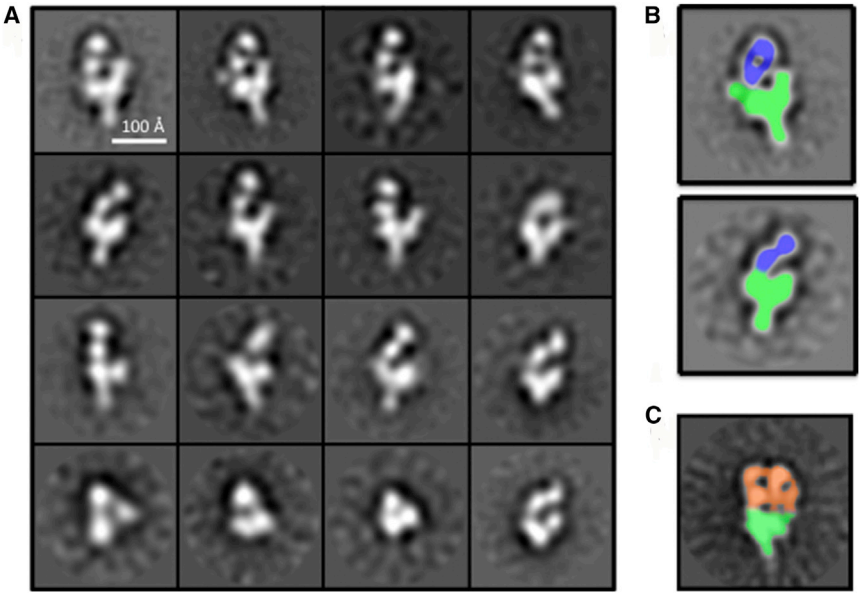

Figure 3. Single-Particle Negative-Stain EM Analysis of FVM04 Fab Bound to EBOV GPΔMuc

(A) Reference-free 2D class averages of the complex illustrate that only a single FVM04 Fab binds to the GP trimer near the glycan cap at the trimer apex. Scale bar represents 100 Å.

(B) Two exemplar class averages have been colored to highlight FVM04 (blue) and the GP trimer (green).

(C) Example class average of the glycan-cap-binding antibody c13C6 (orange) (Murin et al., 2014) that also binds at the GP trimer (green) apex. Relative to c13C6, FVM04 binds closer to the trimer 3-fold axis and is bent inward.

See also Figures S3 and S4.

EBOV GP (GP_{CL}) to its endosomal receptor NPC1. Binding of FLAG-tagged soluble NPC1 domain C to biotinylated VSV-EBOV GP_{CL} immobilized on streptavidin-coated plates was tested in the presence and absence of FVM04. As shown in Figure 4F, FVM04 exhibited concentration-dependent inhibition of NPC-1 binding to GP_{CL}, suggesting that the inhibition of GP binding to its endosomal receptor is one likely mechanism of action for FVM04.

Affinity Measurements

We used biolayer interferometry (BLI) to measure the affinity of FVM04 binding to EBOV, SUDV, or BDBV GP ectodomains (GPΔTM). FVM04 was bound to protein G sensors and exposed to a range of GPΔTM concentrations (Figure 5). The association and dissociation of FVM04 to EBOV and SUDV GPΔTM fit a 1:1 binding model (Figures 5A and 5B). The K_D for EBOV GPΔTM was calculated to be 2.2 ± 0.1 nM, with a k_a (association rate) of (2.5 ± 0.1) × 10^4/M sec and a k_d (dissociation rate) of (5.4 ± 0.1) × 10^{-5}/s. The affinity of FVM04 for SUDV GPΔTM was slightly higher, with a K_D of 9.1 ± 0.2 nM, a k_a of (6.0 ± 0.1) × 10^4/M sec, and a k_d of (5.4 ± 0.1) × 10^{-4}/s. The affinity of FVM04 to EBOV and SUDV GPΔTM was also analyzed in an additional experiment using anti-human Fc-coated sensors, and the K_D values were found to be similar. Interestingly, the binding of FVM04 to BDBV GPΔTM was best described with a 2:1 binding model, with two dissociation constants of $K_D{}^1$ = 570 ± 50 nM and $K_D{}^2$ = 31 ± 1 nM (Figure 5C). The initial association with FVM04 is within the same range of EBOV GPΔTM and SUDV GPΔTM, with a $k_a{}^1$ of (3.8 ± 0.1) × 10^4/M sec, but the second association step is 4-fold slower, with a $k_a{}^2$ of (1.1 ± 0.1) × 10^4/M sec. The dissociation rate of BDBV GPΔTM from FVM04 is the fastest among all three proteins, with a $k_d{}^1$ of (2.2 ± 0.1) × 10^{-2}/s, and a $k_d{}^2$ of (3.3 ± 0.1) × 10^{-4}/s. Collectively, this kinetics analysis offers a biophysical explanation for the differential neutralization profiles between the three viruses. FVM04 exhibits potent neutralization of both EBOV and SUDV, consistent with a high affinity for both glycoproteins in vitro (nanomolar range, K_D), but only a modest neutralization activity against BDBV consistent with poorer binding profiles toward this GP. The difference in binding between EBOV/SUDV and BDBV GP is most evident in the biphasic dissociation phase for BDBV, which is dominated by a dissociation rate (k_d) that is two orders of magnitude faster than for EBOV or SUDV GP.

Efficacy in Mice

We previously reported the efficacy of FVM04 in a mouse model of EBOV when administered at two doses starting immediately after infection (Keck et al., 2015). Here, we expanded these studies to post-exposure treatment in both the EBOV model and a recently developed mouse model for SUDV (Brannan et al., 2015). First, we evaluated the delayed administration of a single dose of FVM04. Groups of ten mice were infected with 100 plaque-forming units (PFU) of mouse-adapted EBOV (MA-EBOV) (Bray et al., 1999) and treated with a single intraperitoneal (i.p.) injection of 10 mg/kg (200 μg per mouse) of FVM04 either 1, 2, or 3 dpi. A single injection of FVM04 at 1 dpi led to full protection from lethal challenge ($p < 0.0001$; determined by Manel-Cox method), while delayed treatment on day 2 or day 3 (peak of viremia) resulted in 80% ($p = 0.0012$) and 30% ($p = 0.108$) protection, respectively (Figure 6A). Consistent with survival data, mice treated at 1 dpi showed no weight loss or sign of disease (Figure 6A). Mice treated on 2 or 3 dpi lost a maximum of 8% and 10% body weight, respectively, compared to 18% weight loss in the control group, and milder clinical signs of disease were observed (Figure 6A). Then, we evaluated the dose response by treating the mice 2 dpi with 10, 5, or 2.5 mg/kg (200, 100, or 50 μg per mouse) of FVM04 or PBS as control. In this study, both 10 and 5 mg/kg FVM04 provided full protection ($p < 0.0001$), while 70% of the mice receiving 2.5 mg/kg survived the challenge ($p = 0.0004$) (Figure 6B). PBS-treated mice lost about 13% of their body weight before succumbing to infection, while mice treated with FVM04 showed less weight loss and less severe disease, as determined by health scores (Figure 6B). These data clearly indicate the post-exposure efficacy of FVM04 at relatively low doses.

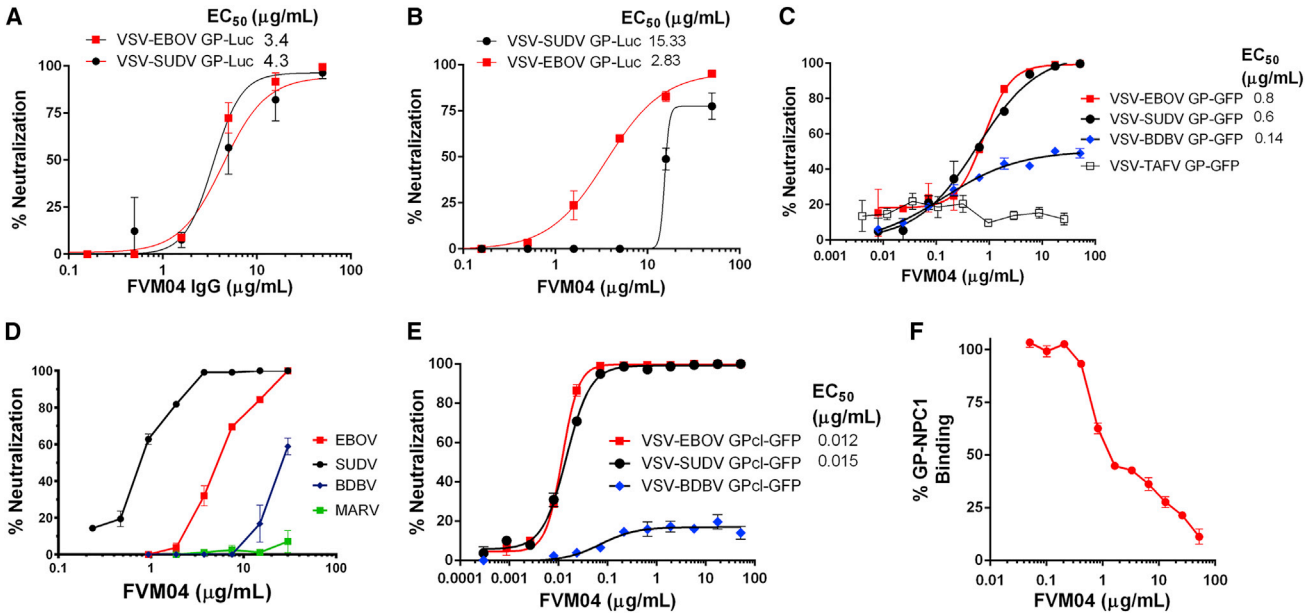

Figure 4. Neutralization of Filoviruses and Inhibition of EBOV GP/NPC-1 Interaction by FVM04

(A) FVM04 was preincubated at different concentrations with VSV-EBOV GP-Luc or VSV-SUDV GP-Luc and added to Vero cells in 96-well plates. Luciferase activity was measured after 48 hr and percent neutralization was calculated in comparison with untreated virus.

(B) Neutralization assay was performed as in (A) using purified FVM04 Fab fragment.

(C) Neutralization of rVSV-GFP expressing full-length GP of EBOV, SUDV, or TAFV, or GPΔMuc of BDBV.

(D) Plaque reduction neutralization of wild-type EBOV, SUDV, BDBV, or MARV by FVM04.

(E) Neutralization of VSV-EBOVGP$_{CL}$ and VSV-SUDVGP$_{CL}$ by FVM04.

(F) VSV-EBOVGP$_{CL}$ was immobilized on streptavidin-coated plates and incubated with Flag-NPC1 in the presence or absence of various concentrations of FVM04. Bound NPC1 was detected using anti-Flag antibody-HRP conjugate. The relative binding of NPC1 was calculated in the presence of inhibiting antibody in comparison to the no-antibody control and plotted as percent binding.

Error bars represent SEM.

Efficacy of FVM04 was further tested in mice in which the genes for IFNα/IFNβ (interferon beta) receptor are knocked out (IFNαβR$^{-/-}$) (Brannan et al., 2015). Groups of seven 4-week-old IFNαβR$^{-/-}$ mice were infected with 1,000 PFU of SUDV followed by i.p. injection of 10 mg/kg of anti-SUDV GP mAb 16F6 at 1 and 3 dpi, or FVM04 at 1 dpi. A control group of six mice received no treatment after the infection. The SUDV-specific 16F6 fully protected mice with minimal weight loss or signs of disease (Figure 6C). Five out of seven mice treated with FVM04 were protected from lethal challenge, while the effect on average weight loss and health scores was not apparent (Figure 6C).

Efficacy in Guinea Pigs

Efficacy of FVM04 was also examined in guinea pigs using guinea-pig-adapted EBOV and SUDV (GPA-EBOV and GPA-SUDV, respectively) (Volchkov et al., 2000; Wong et al., 2015). Four groups of six guinea pigs were challenged with either 1,000 × LD_{50} (the median lethal dose) of GPA-SUDV or GPA-EBOV followed by a single i.p. injection of 5 mg FVM04 (~15 mg/kg) or vehicle control at 1 dpi. Animals were monitored for 16 days for weight change and 28 days for survival. A single injection of FVM04 protected all guinea pigs from GPA-SUDV challenge, while the controls succumbed to infection within 10–13 days ($p = 0.0004$) (Figure 7A). While the controls lost up to 40% body weight after the GPA-SUDV challenge, no weight loss or sign of disease was observed among FVM04-treated animals (Figure 7A). All DPBS-treated guinea pigs infected with GPA-EBOV succumbed to infection within 6–7 days, while two out of six FVM04-treated animals survived the challenge, and the remaining died between 9 and 11 dpi ($p = 0.0012$) (Figure 7B). The median survival was 7 days for the control group and 11 days for the FVM04-treated group. Control animals lost over 25% of their weight before dying, while the FVM04-treated animals initially gained weight followed by a moderate weight loss (~5%) 10–15 days post-challenge (Figure 7B).

The partial protection against EBOV is consistent with previous reports indicating that an antibody cocktail is required for effective post-exposure protection against EBOV in guinea pigs and NHPs (Qiu et al., 2014). ZMapp™, consisting of the two base binders c2G4 and c4G7 and the glycan cap binder c13C6, was selected for testing in NHPs based on significant, but partial, protection in guinea pigs (four out of six) when administered once at 3 dpi (Qiu et al., 2014). Based on the aforementioned study, we hypothesized that replacing one of the ZMapp™ components with FVM04 would lead to an effective EBOV cocktail that is also protective against SUDV. We selected the mAb c4G7 to be replaced, since it binds to an epitope closely overlapping the c2G4 epitope (Audet et al., 2014; Davidson et al., 2015; Murin et al., 2014). First, we tested whether FVM04 alone (5 mg) or a cocktail of c2G4/c13C6/cFVM04 (1.6 mg each) would

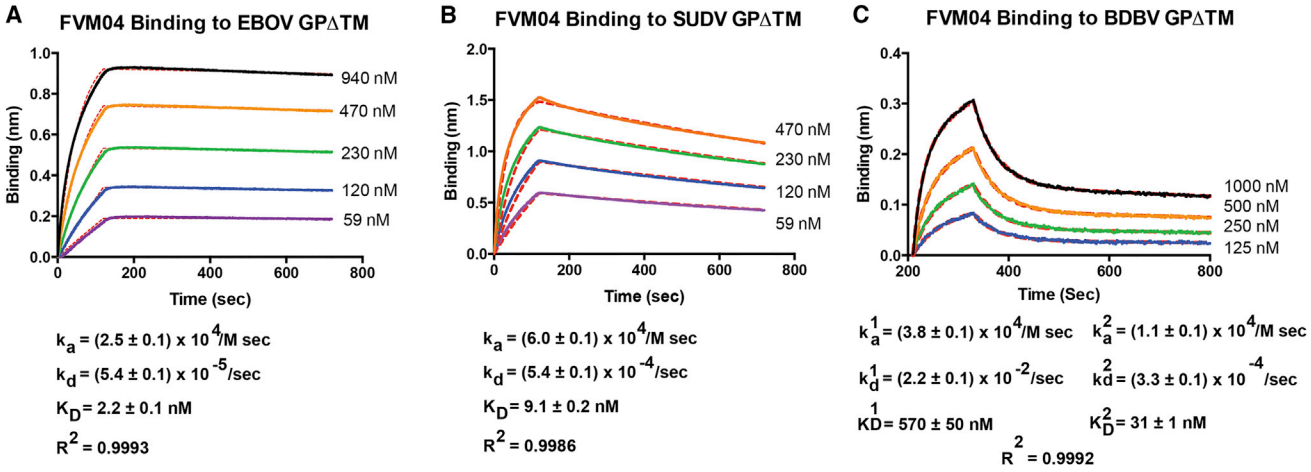

Figure 5. Kinetic Analysis of FVM04 Binding to GP

(A–C) The sensograms show the association and dissociation of EBOV (A), SUDV (B), or BDBV (C) GPΔTM binding to FVM04 immobilized on protein G sensors. Binding to EBOV GPΔTM and SUDV GPΔTM fit to a 1:1 binding model, whereas BDBV GPΔTM fit to a 2:1 binding model. Analyzed concentration ranges are indicated (colored), and the fits are shown as red dashes. On-rate, off-rate, and K_D values for each of the three proteins are shown below the sensograms.

protect against GPA-SUDV when administered at 3 dpi. While all GPA-SUDV-infected control animals died within 10–14 days, all FVM04-treated animals and five out of six animals treated with the cocktail survived the challenge (Figure 7C). The protection was highly significant, with p = 0.0008 for both treatment groups compared with the controls. Animals treated with FVM04 exhibited no weight loss, while control animals lost an average of 25% body weight (Figure 7C). While the animals treated with the cocktail also showed no weight loss on average (Figure 7C), the only fatal case in this group lost 17% of its body weight before dying on day 14 post-infection.

The cocktail consisting of FVM04, c13C6, and c2G4 was also tested in the GPA-EBOV model. Four out of six animals treated with a single dose of 5 mg cocktail (~1.6 mg of each component) at 3 dpi survived the challenge, while all control animals succumbed to infection within 7–9 days (p = 0.0061) (Figure 7D). The control animals lost an average of 20% of their weight, while the average weight within the cocktail-treated group showed a steady increase over 16 dpi (Figure 7D). Of the two cocktail-treated animals that died, one lost about 9% body weight by the day of death (7 dpi), and the second animal actually gained 12% body weight before dying on day 8. As a comparison, Figure 7E shows compiled survival and weight loss data from three studies that we have performed with ZMapp™ (5 mg per animal; n = 20). A survival rate of 67% in guinea pigs for the cocktail of FVM04/c13C6/c2G4 is well within the range of protection afforded by ZMapp™, as shown here and reported previously (Qiu et al., 2014).

DISCUSSION

The devastating 2014 EVD epidemic in West Africa is a sobering reminder of the global threat of filovirus infections. This outbreak reached unprecedented dimensions, despite the fact that the majority of efforts to develop vaccines and therapeutics over the past decade was focused on the same ebolavirus that caused this epidemic. Given the uncertainties about the natural reservoir and the zoonotic dynamics of filoviruses, it is impossible to predict the species or location of future outbreaks. Thus, broadly protective vaccines and therapeutics are urgently needed to cope with this emerging threat. Recent reports indicate that mAbs against GP are effective as post-exposure treatments for ebolavirus hemorrhagic fever (Pettitt et al., 2013; Qiu et al., 2014). ZMapp™, a cocktail of three mAbs against EBOV GP, is among the most advanced therapeutic candidates and has exhibited remarkable efficacy in symptomatic EBOV-infected NHPs (Qiu et al., 2014). However, these immunotherapeutic candidates are species specific and mostly target EBOV (Zaire) only.

According to the current dogma in the field, a combination of antibodies is required for effective control of EBOV infection, and antibodies in current cocktails include those that target the base of the trimeric GP, as well as those that bind the apex of the trimer in the glycan cap (Murin et al., 2014). Recently, engineered bispecific antibodies targeting the GP base of both EBOV and SUDV were shown to provide post-exposure protection in mice (Frei et al., 2016). Despite the structural overlap of 16F6 (SUDV-specific) and KZ52 (EBOV-specific) to date, no cross-binding antibody that targets the GP base epitope on a canonical IgG framework has been described. Thus, antibody cocktails with expanded neutralizing and protective breadth are likely to engage novel epitopes. We have recently identified a set of pan-ebolavirus and pan-filovirus mAbs that target phylogenetically conserved sites within the glycan cap and core GP1, including two mAbs (m8C4 and FVM04) that effectively cross-neutralize EBOV and SUDV, the two most divergent filoviruses (Holtsberg et al., 2015; Keck et al., 2015). Here, we report full characterization of the pan-ebolavirus mAb FVM04 and demonstrate that it targets a uniquely exposed epitope within the RBS and conveys post-exposure protection against both EBOV and SUDV.

The receptor-binding unit of filovirus GP has an ocean-wave morphology with a recessed trough and a rising crest (Bornholdt

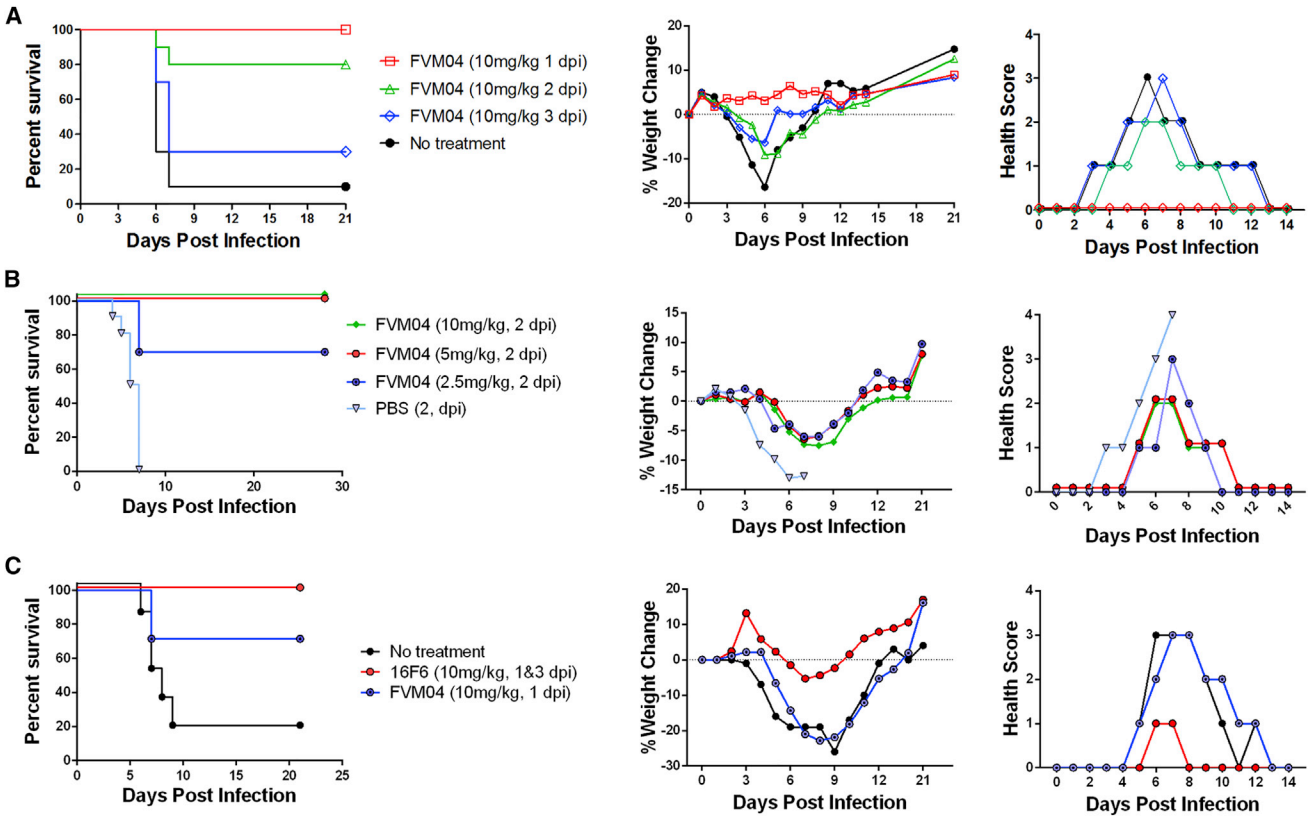

Figure 6. Post-exposure Efficacy of FVM04 in a Mouse Model of EBOV and SUDV Infection

(A and B) Groups of ten BALB/c mice were infected intraperitoneally with 100 PFU of MA-EBOV and treated intraperitoneally with the doses and at time points indicated in the figure or left untreated.

(C) Three groups of IFNαβR$^{-/-}$ mice were infected with 1,000 PFU of SUDV; one group (n = 7) received two i.p. injections of 16F6 at 1 and 3 dpi, a second group received FVM04 once at 1 dpi, and a third group was left untreated. Mice were monitored for 21 days for survival, weight change, and signs of disease.

et al., 2016; Hashiguchi et al., 2015; Wang et al., 2016). The surface of the trough is lined with hydrophobic residues from α1 and β4 strands and their connecting loop in ebolavirus GP and residues 63–74 of MARV GP (Bornholdt et al., 2016; Hashiguchi et al., 2015). In contrast, the wave crest (strands β7 and β9 and their connecting loops in ebolavirus GP) is hydrophilic and contains basic residues that undergo electrostatic interactions with the filovirus host receptor NPC-1 (Bornholdt et al., 2016; Wang et al., 2016). The recessed trough is occluded by specific interaction of residues from the glycan cap, with the hydrophobic lining of the trough blocking its accessibility on the surface of EBOV GP (Hashiguchi et al., 2015). Only after cathepsin-mediated cleavage within endosomes removes the glycan cap are the residues within the ebolavirus GP trough unmasked for specific interaction with NPC1 (Bornholdt et al., 2016; Krishnan et al., 2012; Miller et al., 2012). These findings provide a structural explanation for the observation that MARV-neutralizing antibodies such as MR78 and MR72 (Flyak et al., 2015) bind full-length MARV GP, in which the trough is apparently exposed, but bind and neutralize EBOV only after thermolysin cleavage and removal of the glycan cap (Hashiguchi et al., 2015). In contrast, the tip of the crest is accessible on the surface of GP trimer (Bornholdt et al., 2016; Hashiguchi et al., 2015). Our alanine-scanning mutagenesis analysis reveals K115, D117, and G118 (positioned at the tip of the crest) as critical residues for FVM04 binding. Bornholdt et al. recently demonstrated that mutations of K114 and K115 to alanine significantly reduce NPC-1 binding by GP_{CL}, while mutating these residues to glutamic acid completely abrogates GP interactions with NPC-1, suggesting that these basic residues are involved in receptor binding (Bornholdt et al., 2016). Moreover, the recently solved X-ray crystal structure of a GP_{CL}-NPC-1 domain C protein complex reveals that a loop in NPC1 domain C directly contacts the basic crest (Wang et al., 2016). Here, we show that FVM04 binding specifically blocks the interaction of GP_{CL} with NPC-1. Lately, Corti et al. (2016) also reported an EBOV-specific antibody that binds to the EBOV GP glycan cap and the RBS region and blocks GP interaction with NPC-1 (Misasi et al., 2016). Thus, FVM04 represents a distinct cross-neutralizing antibody that binds an exposed epitope within the ebolavirus RBS and neutralizes the virus, at least in part, through blockade of receptor interaction.

The primary amino acid sequence of the crest region is highly conserved among all ebolaviruses and modestly homologous between ebolaviruses and marburgviruses. The tip of the crest, which includes FVM04 binding sites, also shows high structural homology between EBOV and SUDV and, to a lesser extent,

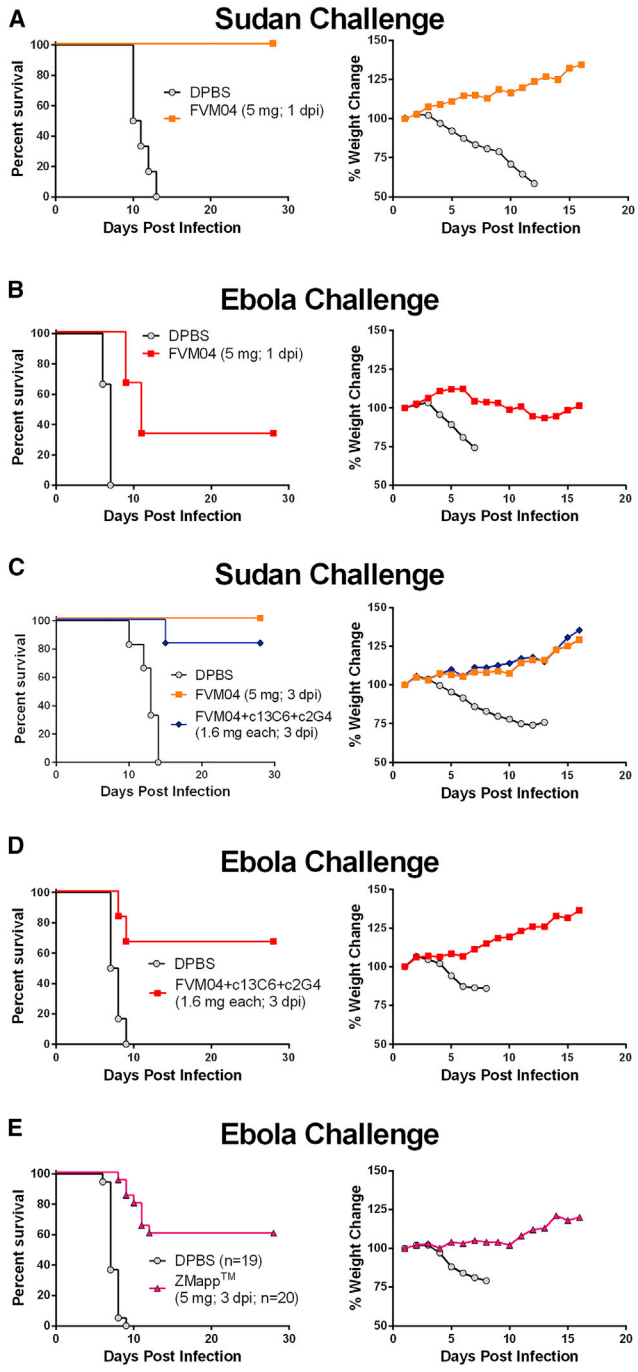

Figure 7. Efficacy of FVM04 Treatment and an FVM04-Containing Cocktail in Guinea Pig Models of SUDV and EBOV Infection

(A and B) Efficacy of a single i.p. dose of 5 mg per animal FVM04 (~15 mg/kg) injected at 1 dpi compared to control group receiving DPBS in animals challenged with GPA-SUDV (A) or GPA-EBOV (B), with six animals per group.

(C) Groups of six guinea pigs were challenged with GPA-SUDV and treated with either DPBS; 5 mg per animal of FVM04; or 1.6 mg per animal each of FVM04, c2G4, and c13C6 at 3 dpi.

(D) Guinea pigs (six animals per group) were infected with GPA-EBOV and treated with 1.6 mg per animal each of FVM04, c2G4, and c13C6 at 3 dpi.

(E) Compiled data of three experiments with ZMapp™. Guinea pigs were infected with GPA-EBOV and treated with DPBS (n = 19) or 5 mg per animal of ZMapp™ (n = 20) at 3 dpi. Challenge was performed with 1,000 × LD_{50} of GPA-SUDV or GPA-EBOV as indicated. Survival was monitored for 21 dpi, and weights were monitored for 16 days dpi.

between EBOV and MARV GP. While FVM04 effectively neutralized both EBOV and SUDV, it only exhibited partial neutralization of BDBV. Our previous results indicated that FVM04 binds to BDBV GP with an ELISA EC_{50} comparable to those of EBOV and SUDV (Keck et al., 2015). However, our kinetic analysis in this report showed that FVM04 has a very rapid off rate for BDBV GP, providing a possible explanation for low neutralizing activity toward BDBV. The amino acid sequence of the EBOV and BDBV GP crest regions only differ in positions 112 (glutamic acid in EBOV versus aspartic acid in BDBV) and 116 (proline in EBOV versus alanine in BDBV). In our alanine-scanning analysis, the E112A and P116A mutations in EBOV GP did not alter the binding to FVM04 (106% and 115% of wild-type respectively). However, it is possible that the residues 112 and 116 influence the positioning of the key residues 115, 117, and 118 or are part of the epitope directly but at a lower energetic level that cannot be captured by the cell-surface staining assay. FVM04 did not neutralize VSV pseudotyped with TAFV GP, which also differs from EBOV GP in the same crest residues as BDBV with alanine and valine in positions 112 and 116, respectively. Nonetheless, FVM04 is an effective neutralizer of the most virulent ebolaviruses EBOV and SUDV.

An interesting feature of FVM04 is its asymmetric binding to GP in contrast to antibodies such as ZMapp™ components (Murin et al., 2014) and KZ52 (Lee et al., 2008). Class averages from the analysis of negative-stain EM of FVM04 Fab bound to GPΔMuc revealed that it binds with a stoichiometry of one Fab per trimer. The position of FVM04 in EM studies is consistent with the mutational analysis. Together, these results suggest that this mAb binds with a more angled pose than c13C6, which binds at the top of GP as well but perpendicular to the plane of the viral membrane (Murin et al., 2014). Although we have not quantitatively established with solution studies that only a single FVM04 Fab is capable of binding, even at saturating concentrations, it seems reasonable from the EM-derived images that the angle of approach for a single FVM04 Fab occludes the other potential binding sites on the other two subunits. Further studies are required to elucidate the implications of this binding morphology on neutralization and in vivo efficacy, but a tantalizing possibility is that fewer FVM04 IgG molecules bind the GP trimer than other IgGs on average. Lower requirement for occupancy could, in theory, provide a therapeutic advantage because less antibody would be required for neutralization and render the IgG less susceptible to decoy antigens such as sGP or GP spike on defective particles. For example, studies performed with anti-EBOV equine Ig clearly showed rapid reduction in EBOV-specific equine IgG titer during the peak of viremia in NHPs, while total equine IgG titer remained constant (Jahrling et al., 1996), suggesting high antibody consumption during infection. Single-site occupancy could also potentially leave more of the GP surface exposed in the mAb-GP complex, providing additional opportunities for engagement of other epitopes by other antibodies in a cocktail.

While the FVM04 epitope is accessible, the binding is probably not entirely free of steric hindrance. Our previous report indicated

that FVM04 binding to GP was slightly increased after removal of MLD and the glycan cap (Keck et al., 2015), and data in Figure 4E show that FVM04 neutralizes the virus carrying GP_{CL} more effectively than full-length GP. Interestingly, our mutagenesis studies revealed that, in contrast to KZ52, binding of FVM04 was substantially enhanced when certain residues within the base of the GP (GP2 and N terminus of GP1) were mutated to alanine. Most of these mutations also increased binding of other cross-reactive antibodies that we had previously reported (Holtsberg et al., 2015; Keck et al., 2015), such as 4B8, m8C4, FVM09, and FVM20. These residues are mostly hydrophobic and buried in the structure, suggesting that single-point mutations within the base may loosen up the apex, exposing cross-reactive epitopes. This finding may have important implications for the development of pan-ebolavirus vaccines if such mutations can be incorporated into vaccines to improve their potency or breadth of protection.

Efficacy studies in mice and guinea pigs showed the high therapeutic value of FVM04. Full protection from EBOV infection was observed 2 dpi with as little as 100 μg per mouse, and a lower dose of 50 μg per mouse showed partial but significant protection. A small-scale study in $IFN\alpha\beta R^{-/-}$ mice showed 71% protection from lethal SUDV challenge when FVM04 was administered 1 dpi. These data show that FVM04 compares well with the post-exposure efficacy (2 dpi) of EBOV-specific mAbs 1H3, 2G4, and 4G7 as reported (Qiu et al., 2012b), while expanding the breadth of protection to include SUDV.

The guinea pig model of EBOV infection is considered a substantially more stringent model for screening of therapeutics (Cross et al., 2015; Parren et al., 2002; Qiu et al., 2012b), Particularly, the testing of therapeutics at 3 dpi in this model is particularly stringent, with good predictive value for efficacy in NHPs (Qiu et al., 2014). Recently, Wong et al. also reported the development of a guinea pig model of SUDV infection (Wong et al., 2015). The GPA-SUDV causes a uniformly lethal infection, with the major hallmarks of SUDV infection, including lymphadenopathy, increased liver enzyme activities, and coagulation abnormalities (Wong et al., 2015). We used both of these models in the present study to evaluate the efficacy of FVM04.

A single injection of FVM04 (5 mg) at 1 or 3 dpi fully protected guinea pigs against GPA-SUDV infection with no signs of disease. This suggests that FVM04 alone may be sufficient to control SUDV infection. To date, no SUDV antibodies have been tested in NHP studies; thus, it is not known how protection in rodent models relates to efficacy against SUDV in NHPs. In contrast, in the EBOV guinea pig model, a protection level of more than ~60%, 3 dpi, at a total dose of 5 mg is a good indicator of efficacy in NHPs. In fact, the ZMapp™ cocktail that fully protected NHPs at 5 dpi was selected based on partial efficacy at 3 dpi in guinea pigs (Qiu et al., 2014). In the GPA-EBOV-infected guinea pigs, FVM04 protected two out of six animals when administered at 1 dpi. While the protection level of 33% was statistically significant, it was lower than the reported protection level of 60% at 1 dpi afforded by c2G4 or c4G7 (Qiu et al., 2012b). These data suggested that, while FVM04 alone may be sufficient for SUDV, more efficient protection against EBOV would require a cocktail. Given that c2G4 and c4G7 target overlapping epitopes (Murin et al., 2014), we reasoned that 4G7 may be a good candidate for replacement by FVM04. This led to a cocktail of FVM04/c2G4/c13C6 that protected five out of six guinea pigs against SUDV and four out of six animals against EBOV. This level of protection against EBOV is comparable with historical efficacy data of ZMapp™ (Figure 7E) (Qiu et al., 2014). These data demonstrate that a cocktail of FVM04, c13C6, and c2G4, is as effective as ZMapp™ against EBOV while expanding the breadth of protection to include SUDV. The efficacy of these cocktails must be further tested in future NHP studies; however, these data position FVM04 as a strong candidate to be a component of a pan-ebolavirus therapeutic cocktail.

EXPERIMENTAL PROCEDURES

Antibody Production

FVM04 was produced in HEK293 cells transfected with the plasmid encoding IgH and IgL using polyethylenimine (Polysciences) and purified by protein A chromatography, as described previously (Keck et al., 2015). For ZMapp™ production, *N. benthamiana* plants genetically modified to produce homogenous mammalian N-glycans of the GnGn glycoform were grown for 4 weeks in an enclosed growth room (20–23°C) and used for vacuum infiltration as described previously (Hiatt et al., 2014). Seven days later, the mAb was extracted from the leaf tissue and purified via protein A chromatography, and endotoxin was removed using an Acrodisc Unit with Mustang Q Membrane (Pall Life Sciences). For Fab production, FVM04 IgG was incubated in 2% papain for 2 hr at 37°C, and the reaction was quenched with 50 mM iodoacetamide. The Fc portion was removed via protein A affinity, and the Fab was further purified via S75 SEC.

Shotgun Mutagenesis Epitope Mapping

Alanine-scanning mutagenesis of an expression construct for full-length EBOV GP (strain Mayinga-76) (Davidson et al., 2015) changed residues 33–676 to alanine (and alanine residues to serine) to create a library of clones, each representing an individual point mutant, covering 641 of 644 residues. Clones were individually arrayed into 384-well plates, transfected into HEK293T cells, and allowed to express for 22 hr. Cells were incubated with primary antibody and then with an Alexa-Fluor-488-conjugated secondary antibody (Jackson ImmunoResearch Laboratories). After washing, cellular fluorescence was detected using the Intellicyt high-throughput flow cytometer (Intellicyt). Background fluorescence was determined in vector-transfected control cells. mAb reactivity against each mutant GP clone was calculated relative to wild-type GP reactivity by subtracting the signal from mock-transfected controls and normalizing to the signal from wild-type GP-transfected controls. Mutated residues within clones were identified as critical to a test mAb epitope if they did not support reactivity of the mAb but did support the reactivity of other control EBOV mAbs. This counter-screen facilitates the exclusion of GP mutants that are locally misfolded or have an expression defect. The detailed algorithms used to interpret shotgun mutagenesis data are described elsewhere (patent application 61/938,894; Davidson and Doranz, 2014).

Cell Lines

All cell lines were obtained from ATCC. Vero and HEK293T cells were maintained in DMEM (Life Technologies) and supplemented with 10% fetal bovine serum (FBS) (Atlanta Biologicals) and 1% penicillin-streptomycin (Life Technologies). BHK-21 and Vero cells were grown in Eagle's minimal essential medium (EMEM) (Corning) supplemented with 10% FBS and 1% penicillin-streptomycin. All cell lines were maintained in a humidified 37°C, 5% CO_2 incubator.

Negative-Stain EM Studies

EBOV GPΔMuc and FVM04 were each individually purified. EBOV GPΔMuc was combined with a 10-fold molar excess of FVM04 Fab and incubated overnight at 4°C. The complex was further purified by SEC with an S200i column (GE Healthcare) equilibrated in Tris-buffered saline (TBS). The complex was deposited onto a carbon-coated 400 copper mesh grid and subsequently stained with 1% uranyl formate. Grids were loaded into a Tecnai T12 Spirit at 120keV

and imaged using this Tietz TemCam-F416 CMOS camera at 52,000× magnification at a nominal defocus of ~1.5 μM. Micrographs were collected automatically using Leginon (Suloway et al., 2005) and processed within Appion (Lander et al., 2009). DogPicker (Voss et al., 2009) was used to automatically pick particles in the raw micrographs and placed into a 2D stack. Initial reference-free 2D classification was undertaken in XMIPP (Sorzano et al., 2004), and particles that did not correspond to EBOV GPΔMuc bound to FVM04 (e.g., noise or amorphous particles) were removed at this point, resulting in a final stack of 13,139 particles. The remaining 13,139 particles were then processed in two subsequent rounds of reference-free 2D classification in Relion 1.4 (Scheres, 2012), resulting in a final particle count of 8,208. Approximately half of the final 2D class averages had identifiable complexes of EBOV GPΔMuc bound to FVM04. Images were created in UCSF Chimera and Adobe Photoshop.

SEC-MALS

To determine the absolute molecular weight of EBOV GPΔmuc, we first performed SEC-MALS using conjugate analysis to account for glycan content. To determine the number of FVM04 Fab molecules bound to EBOV GPΔmuc trimer, SEC-MALS was repeated with EBOV GPΔmuc that had been complexed with excess FVM04 Fab for 6 hr at room temperature. A Superdex 200 SEC column was coupled in line with the following calibrated detectors: (1) a MiniDawn Treos MALS detector (Wyatt Corporation) and (2) an Optilab T-reX refractive index (RI) detector (Wyatt Corporation). The Astra VI software (Wyatt Corporation) was used to combine these measurements to determine the absolute molar mass of the eluted proteins.

Neutralization Assays

Two different neutralization assays based on pseudotyped recombinant VSV-expressing filovirus GP were used: a replication-defective recombinant Indiana VSV (rVSV)-GP-Luc expressing firefly luciferase and a replication-competent rVSV expressing GFP (rVSV-GFP).

rVSV-GP Luciferase Pseudotype Assay

Pseudotyped viruses were generated based on a modification of a previously published method (Whitt, 2010). HEK293T cells (80% confluency) were transfected with plasmids encoding EBOV GP, MARV GP, or SUDV GP using Fugene HD (Promega) according to the manufacturer's protocol. The next day, these cells were infected with rVSV-ΔGP pseudotype (Kerafast) at an MOI of 3, and the virus was washed off after 1 hr with DPBS. The next day, the supernatant was collected and clarified by centrifugation. To titer the pseudotyped virus, BHK-21 cells were transfected in six-well plates with pCAGGS VSV-G (Kerafast), and after 48 hr, serial dilution of VSV-EBOV-GP-Luc or VSV-SUDV-GP-Luc pseudotype was added to each well for 1 hr before the addition of 0.9% agar in DMEM. The next day, wells were fixed with 5% glutaraldehyde for 30 min before removing the agar and staining with crystal violet to count the plaques. The details of the luciferase assay for the determination of VSV-GP-Luc infectivity were previously described (Keck et al., 2015). Data were fit to a 4PL curve using GraphPad Prism 6. Percent neutralization was calculated based on wells containing virus only.

rVSV GP-GFP Assay

rVSVs expressing EGFP, as well as EBOV or MARV GP in place of VSV-G, were described previously (Miller et al., 2012; Ng et al., 2014; Wong et al., 2010). rVSVs bearing TAFV, SUDV GP, or BDBV GPΔMuc were generated by the same method. VSV particles containing cleaved GP (GP_{CL}) were generated by incubating rVSV-GPs with thermolysin (200 μg/ml) for 1 hr at 37°C, followed by treatment with phosphoramidon (1 mM), and reaction mixtures were used immediately. Infectivity of rVSVs was measured by counting EGFP-positive cells at 12–14 hr post-infection using a CellInsight CX5 automated microscope and onboard software (Thermo Scientific). For neutralization experiments, serial dilutions of mAbs were incubated with the rVSV-GP for 1 hr at room temperature. Monolayers of Vero cells seeded in 96-well plates were inoculated with the mAb-virus mixture in triplicate and then incubated at 37°C overnight. Infection was scored 12 hr to 16 hr post-infection by the enumeration of $eGFP^+$ cells and normalized to no-antibody control taken to represent 100%.

PRNT Assay

Antibody at indicated concentrations was incubated with 100 PFU of EBOV (Kikwit-95) or SUDV (Boniface) at 37°C, 5% CO_2, and 80% humidity for 1 hr. The mixture was then added to Vero cells in six-well plates and incubated for 1 hr. Cells were then overlaid with a mixture of one part 1% agarose (Seakem) and one part 2X Eagle's basal medium (EBME), 30 mM HEPES buffer, and 5% ΔFBS and incubated at 37°C, 5% CO_2, and 80% humidity. A second overlay containing 5% neutral red was added 6–7 days later, and plates were incubated overnight. Plaques were counted the following day, and percent neutralization was determined by comparing to control wells.

Antibody-Mediated Inhibition of EBOV GP-NPC1 Binding

Thermolysin-cleaved VSV-GP (rVSV-GP_{CL}) was incubated with a functional-spacer-lipid reagent conjugated to biotin (FSL-biotin; Sigma) to allow incorporation into viral membrane, and the resulting biotinylated viral particles were then captured onto streptavidin-coated plates, as described previously (Ng et al., 2014). Plates were then washed and blocked with 3% BSA-PBS buffer. Serial dilutions of antibodies were added to virus-coated plates, and after washing, soluble FLAG-tagged NPC1 domain C protein (2 nM) was added to each well. Plates were washed, and the extent of NPC1 binding to rVSV-GP_{CL} was detected using an anti-FLAG-HRP (horseradish peroxidase) antibody conjugate. All incubations were performed for 1 hr at 37°C. Binding was expressed as percentage of the maximal binding signal obtained with no-antibody control.

Affinity Measurements Using Octet

Kinetics experiments were performed on the ForteBio Octet Red96 platform. Data were collected at 25°C with orbital shaking at 1,000 rpm in 200 μl. Protein G or Anti-human Fc sensors (ForteBio) were equilibrated in kinetics buffer (1× PBS, 0.1% BSA, and 0.02% Tween-20) for 10 min prior to loading with 10 μg/ml FVM04 antibody for 2 min. A stable baseline was established in kinetics buffer for 1 min before the FVM04-coated sensors were added to a range of EBOV, SUDV, or BDBV GPΔTM concentrations. The association step of GPΔTM with FVM04 proceeded for 2 min before allowing the GPΔTM to dissociate into kinetics buffer for 10 min. A reference sensor without FVM04 was used to account for nonspecific binding of GP to the sensor. The data were fit globally to a 1:1 or 2:1 Langmuir binding model using ForteBio data analysis software 9.0.

Animal Challenge Studies

Mouse Challenge Studies with EBOV

Female BALB/c mice (6–8 weeks old) were purchased from Charles River Laboratories. Mice were exposed to an i.p. dose of 100 PFU of (Mayinga strain) MA-EBOV suspended in PBS. Antibodies were delivered at the indicated i.p. doses and time points after exposure. Control mice were treated with PBS or left untreated. Mice were observed daily for clinical signs of disease, including but not limited to, reduced grooming and hypoactivity, and group weights were recorded through day 14. Observations were increased to a minimum of twice daily when mice exhibited signs of disease. Moribund mice were humanely euthanized based on Institutional Animal Care and Use Committee (IACUC)-approved criteria. Mice were observed a minimum of 21 days after exposure.

Mouse Challenge Study with SUDV

$IFN\alpha\beta R^{-/-}$ mice (4 weeks old) (B6.129S2-Ifnar1tm1Agt/Mmjax) on the C57BL/6 background were purchased from Jackson Laboratories. Upon arrival, mice were housed in microisolater cages and provided chow and water ad libitum. Mice were challenged intraperitoneally with 1,000 PFU of SUDV and treated at indicated times with antibodies by i.p. injection. Mice were observed daily for lethality or clinical signs of disease. Moribund mice were humanely euthanized based on IACUC-approved criteria.

Guinea Pig Challenge Studies

Female Hartley guinea pigs (4–6 weeks old, 250–300 g) were purchased from Charles River Laboratories and randomly assigned into different groups. All guinea pigs were challenged with an i.p. dose of 1,000 × LD_{50} GPA-EBOV (Volchkov et al., 2000) or 1,000 × LD_{50} GPA-SUDV (Wong et al., 2015) in 1 ml DMEM. The mAbs or mAb cocktail were given in an i.p. dose once at 1 or 3 dpi with 5 mg of each individual mAb or mAb cocktail (at a 1:1:1 ratio of each mAb) per animal. The control group was given 1 ml PBS. All animals were monitored for signs of disease, survival, and weight change for 15–16 days, and survival was monitored for 12 additional days.

Ethics Statement

Animal research using mice was conducted under a protocol approved by the U.S. Army Medical Research Institute of Infectious Diseases (USAMRIID) IACUC in compliance with the Animal Welfare Act and other federal statutes and regulations relating to animals and experiments involving animals. The USAMRIID facility is fully accredited by the Association for the Assessment and Accreditation of Laboratory Animal Care International and adheres to the principles stated in the Guide for the Care and Use of Laboratory Animals. Challenge studies were conducted under maximum containment in an animal BSL-4 facility. The guinea pig experiments were performed at the National Microbiology Laboratory in Winnipeg, MB, Canada. All animal experiments have been approved by the Animal Care Committee at the Canadian Science Center for Human and Animal Health in accordance with the guidelines outlined by the Canadian Council on Animal Care.

SUPPLEMENTAL INFORMATION

Supplemental Information includes four figures and one table and can be found with this article online at http://dx.doi.org/10.1016/j.celrep.2016.04.026.

AUTHOR CONTRIBUTIONS

K.A.H., X.Q., J.M.B., C.B., E.D., A.Z.W., S.G.E., E.K.N., Z.-Y.K., S.H., H.V., A.S.H., and A.K. performed characterization, epitope mapping, and animal experiments. F.W.H., S.S., and M.L.F. performed protein and antibody production. H.L.T., J.P., and C.D.M. performed purification of complexes and E.M., F.W.H., J.E.B., R.D., J.R.L., S.K.H.F., E.O.S., L.Z., A.B.W., K.C., B.J.D., G.P.K., J.M.D., and M.J.A. were involved in the design of the experiments. All authors reviewed and analyzed data. M.J.A. and K.A.H. wrote the paper.

ACKNOWLEDGMENTS

This work was supported by a contract (HDTRA1-13-C-0015) from the U.S. Defense Threat Reduction Agency (DTRA) to M.J.A., grant U19 AI109762 from the NIH to E.O.S., and NIH contract HHSN272201400058C to B.J.D. J.R.L. acknowledges funding from the NIH (U19AI109762). This work was also partially supported by the Public Health Agency of Canada (PHAC). We thank Andrew McNeal and Rachel Fong for valuable technical assistance. C.D.M. is supported by a pre-doctoral fellowship from the National Science Foundation. E.K.N. was supported by a DAAD (Deutscher Akademischer Austauschdienst [German Academic Exchange Service]) fellowship. Opinions, interpretations, conclusions, and recommendations are those of the authors and are not necessarily endorsed by the U.S. Army. M.J.A. is a shareholder of Integrated Biotherapeutics. S.G.E., F.W.H., H.V., R.D., and S.S. own stock options in Integrated Biotherapeutics.

Received: February 3, 2016
Revised: March 7, 2016
Accepted: April 3, 2016
Published: May 5, 2016

REFERENCES

Audet, J., Wong, G., Wang, H., Lu, G., Gao, G.F., Kobinger, G., and Qiu, X. (2014). Molecular characterization of the monoclonal antibodies composing ZMAb: a protective cocktail against Ebola virus. Sci. Rep. *4*, 6881.

Bornholdt, Z.A., Ndungo, E., Fusco, M.L., Bale, S., Flyak, A.I., Crowe, J.E., Jr., Chandran, K., and Saphire, E.O. (2016). Host-primed Ebola virus GP exposes a hydrophobic NPC1 receptor-binding pocket, revealing a target for broadly neutralizing antibodies. MBio *7*, e02154-15.

Bounds, C.E., Kwilas, S.A., Kuehne, A.I., Brannan, J.M., Bakken, R.R., Dye, J.M., Hooper, J.W., Dupuy, L.C., Ellefsen, B., Hannaman, D., et al. (2015). Human polyclonal antibodies produced through DNA vaccination of transchromosomal cattle provide mice with post-exposure protection against lethal Zaire and Sudan ebolaviruses. PLoS ONE *10*, e0137786.

Brannan, J.M., Froude, J.W., Prugar, L.I., Bakken, R.R., Zak, S.E., Daye, S.P., Wilhelmsen, C.E., and Dye, J.M. (2015). Interferon α/β receptor-deficient mice as a model for Ebola virus disease. J. Infect. Dis. *212* (*Suppl 2*), S282–S294.

Bray, M., Davis, K., Geisbert, T., Schmaljohn, C., and Huggins, J. (1999). A mouse model for evaluation of prophylaxis and therapy of Ebola hemorrhagic fever. J. Infect. Dis. *179* (*Suppl 1*), S248–S258.

Corti, D., Misasi, J., Mulangu, S., Stanley, D.A., Kanekiyo, M., Wollen, S., Ploquin, A., Doria-Rose, N.A., Staupe, R.P., Bailey, M., et al. (2016). Protective monotherapy against lethal Ebola virus infection by a potently neutralizing antibody. Science *351*, 1339–1342.

Coughlin, M.M., and Prabhakar, B.S. (2012). Neutralizing human monoclonal antibodies to severe acute respiratory syndrome coronavirus: target, mechanism of action, and therapeutic potential. Rev. Med. Virol. *22*, 2–17.

Cross, R.W., Fenton, K.A., Geisbert, J.B., Mire, C.E., and Geisbert, T.W. (2015). Modeling the disease course of Zaire ebolavirus infection in the outbred guinea pig. J. Infect. Dis. *212* (*Suppl 2*), S305–S315.

Davidson, E., and Doranz, B.J. (2014). A high-throughput shotgun mutagenesis approach to mapping B-cell antibody epitopes. Immunology *143*, 13–20.

Davidson, E., Bryan, C., Fong, R.H., Barnes, T., Pfaff, J.M., Mabila, M., Rucker, J.B., and Doranz, B.J. (2015). Mechanism of binding to Ebola virus glycoprotein by the ZMapp, ZMAb, and MB-003 cocktail antibodies. J. Virol. *89*, 10982–10992.

Dias, J.M., Kuehne, A.I., Abelson, D.M., Bale, S., Wong, A.C., Halfmann, P., Muhammad, M.A., Fusco, M.L., Zak, S.E., Kang, E., et al. (2011). A shared structural solution for neutralizing ebolaviruses. Nat. Struct. Mol. Biol. *18*, 1424–1427.

Dye, J.M., Herbert, A.S., Kuehne, A.I., Barth, J.F., Muhammad, M.A., Zak, S.E., Ortiz, R.A., Prugar, L.I., and Pratt, W.D. (2012). Postexposure antibody prophylaxis protects nonhuman primates from filovirus disease. Proc. Natl. Acad. Sci. USA *109*, 5034–5039.

Flyak, A.I., Ilinykh, P.A., Murin, C.D., Garron, T., Shen, X., Fusco, M.L., Hashiguchi, T., Bornholdt, Z.A., Slaughter, J.C., Sapparapu, G., et al. (2015). Mechanism of human antibody-mediated neutralization of Marburg virus. Cell *160*, 893–903.

Flyak, A.I., Shen, X., Murin, C.D., Turner, H.L., David, J.A., Fusco, M.L., Lampley, R., Kose, N., Ilinykh, P.A., Kuzmina, N., et al. (2016). Cross-reactive and potent neutralizing antibody responses in human survivors of natural ebolavirus infection. Cell *164*, 392–405.

Frei, J.C., Nyakatura, E.K., Zak, S.E., Bakken, R.R., Chandran, K., Dye, J.M., and Lai, J.R. (2016). Bispecific antibody affords complete post-exposure protection of mice from both Ebola (Zaire) and Sudan viruses. Sci. Rep. *6*, 19193.

Georgiev, I.S., Gordon Joyce, M., Zhou, T., and Kwong, P.D. (2013). Elicitation of HIV-1-neutralizing antibodies against the CD4-binding site. Curr. Opin. HIV AIDS *8*, 382–392.

Hashiguchi, T., Fusco, M.L., Bornholdt, Z.A., Lee, J.E., Flyak, A.I., Matsuoka, R., Kohda, D., Yanagi, Y., Hammel, M., Crowe, J.E., Jr., and Saphire, E.O. (2015). Structural basis for Marburg virus neutralization by a cross-reactive human antibody. Cell *160*, 904–912.

Hiatt, A., Bohorova, N., Bohorov, O., Goodman, C., Kim, D., Pauly, M.H., Velasco, J., Whaley, K.J., Piedra, P.A., Gilbert, B.E., and Zeitlin, L. (2014). Glycan variants of a respiratory syncytial virus antibody with enhanced effector function and in vivo efficacy. Proc. Natl. Acad. Sci. USA *111*, 5992–5997.

Holtsberg, F.W., Shulenin, S., Vu, H., Howell, K.A., Patel, S.J., Gunn, B., Karim, M., Lai, J.R., Frei, J.C., Nyakatura, E.K., et al. (2015). Pan-ebolavirus and pan-filovirus mouse monoclonal antibodies: protection against Ebola and Sudan viruses. J. Virol. *90*, 266–278.

Jahrling, P.B., Geisbert, J., Swearengen, J.R., Jaax, G.P., Lewis, T., Huggins, J.W., Schmidt, J.J., LeDuc, J.W., and Peters, C.J. (1996). Passive immunization of Ebola virus-infected cynomolgus monkeys with immunoglobulin from hyperimmune horses. Arch. Virol. Suppl. *11*, 135–140.

Keck, Z.Y., Enterlein, S.G., Howell, K.A., Vu, H., Shulenin, S., Warfield, K.L., Froude, J.W., Araghi, N., Douglas, R., Biggins, J., et al. (2015). Macaque

monoclonal antibodies targeting novel conserved epitopes within filovirus glycoprotein. J. Virol. *90*, 279–291.

Krishnan, A., Miller, E.H., Herbert, A.S., Ng, M., Ndungo, E., Whelan, S.P., Dye, J.M., and Chandran, K. (2012). Niemann-Pick C1 (NPC1)/NPC1-like1 chimeras define sequences critical for NPC1's function as a filovirus entry receptor. Viruses *4*, 2471–2484.

Kuhn, J.H., Andersen, K.G., Baize, S., Bào, Y., Bavari, S., Berthet, N., Blinkova, O., Brister, J.R., Clawson, A.N., Fair, J., et al. (2014). Nomenclature- and database-compatible names for the two Ebola virus variants that emerged in Guinea and the Democratic Republic of the Congo in 2014. Viruses *6*, 4760–4799.

Lander, G.C., Stagg, S.M., Voss, N.R., Cheng, A., Fellmann, D., Pulokas, J., Yoshioka, C., Irving, C., Mulder, A., Lau, P.W., et al. (2009). Appion: an integrated, database-driven pipeline to facilitate EM image processing. J. Struct. Biol. *166*, 95–102.

Lee, P.S., and Wilson, I.A. (2015). Structural characterization of viral epitopes recognized by broadly cross-reactive antibodies. Curr. Top. Microbiol. Immunol. *386*, 323–341.

Lee, J.E., Fusco, M.L., Hessell, A.J., Oswald, W.B., Burton, D.R., and Saphire, E.O. (2008). Structure of the Ebola virus glycoprotein bound to an antibody from a human survivor. Nature *454*, 177–182.

Maruyama, T., Rodriguez, L.L., Jahrling, P.B., Sanchez, A., Khan, A.S., Nichol, S.T., Peters, C.J., Parren, P.W., and Burton, D.R. (1999). Ebola virus can be effectively neutralized by antibody produced in natural human infection. J. Virol. *73*, 6024–6030.

Marzi, A., and Feldmann, H. (2014). Ebola virus vaccines: an overview of current approaches. Expert Rev. Vaccines *13*, 521–531.

Marzi, A., Yoshida, R., Miyamoto, H., Ishijima, M., Suzuki, Y., Higuchi, M., Matsuyama, Y., Igarashi, M., Nakayama, E., Kuroda, M., et al. (2012). Protective efficacy of neutralizing monoclonal antibodies in a nonhuman primate model of Ebola hemorrhagic fever. PLoS ONE *7*, e36192.

Miller, E.H., and Chandran, K. (2012). Filovirus entry into cells—new insights. Curr. Opin. Virol. *2*, 206–214.

Miller, E.H., Obernosterer, G., Raaben, M., Herbert, A.S., Deffieu, M.S., Krishnan, A., Ndungo, E., Sandesara, R.G., Carette, J.E., Kuehne, A.I., et al. (2012). Ebola virus entry requires the host-programmed recognition of an intracellular receptor. EMBO J. *31*, 1947–1960.

Misasi, J., Gilman, M.S., Kanekiyo, M., Gui, M., Cagigi, A., Mulangu, S., Corti, D., Ledgerwood, J.E., Lanzavecchia, A., Cunningham, J., et al. (2016). Structural and molecular basis for Ebola virus neutralization by protective human antibodies. Science *351*, 1343–1346.

Murin, C.D., Fusco, M.L., Bornholdt, Z.A., Qiu, X., Olinger, G.G., Zeitlin, L., Kobinger, G.P., Ward, A.B., and Saphire, E.O. (2014). Structures of protective antibodies reveal sites of vulnerability on Ebola virus. Proc. Natl. Acad. Sci. USA *111*, 17182–17187.

Ng, M., Ndungo, E., Jangra, R.K., Cai, Y., Postnikova, E., Radoshitzky, S.R., Dye, J.M., Ramírez de Arellano, E., Negredo, A., Palacios, G., et al. (2014). Cell entry by a novel European filovirus requires host endosomal cysteine proteases and Niemann-Pick C1. Virology *468-470*, 637–646.

Olinger, G.G., Jr., Pettitt, J., Kim, D., Working, C., Bohorov, O., Bratcher, B., Hiatt, E., Hume, S.D., Johnson, A.K., Morton, J., et al. (2012). Delayed treatment of Ebola virus infection with plant-derived monoclonal antibodies provides protection in rhesus macaques. Proc. Natl. Acad. Sci. USA *109*, 18030–18035.

Oswald, W.B., Geisbert, T.W., Davis, K.J., Geisbert, J.B., Sullivan, N.J., Jahrling, P.B., Parren, P.W., and Burton, D.R. (2007). Neutralizing antibody fails to impact the course of Ebola virus infection in monkeys. PLoS Pathog. *3*, e9.

Parren, P.W., Geisbert, T.W., Maruyama, T., Jahrling, P.B., and Burton, D.R. (2002). Pre- and postexposure prophylaxis of Ebola virus infection in an animal model by passive transfer of a neutralizing human antibody. J. Virol. *76*, 6408–6412.

Pettitt, J., Zeitlin, L., Kim, H., Working, C., Johnson, J.C., Bohorov, O., Bratcher, B., Hiatt, E., Hume, S.D., Johnson, A.K., et al. (2013). Therapeutic intervention of Ebola virus infection in rhesus macaques with the MB-003 monoclonal antibody cocktail. Sci. Transl. Med. *5*, 199ra113.

Qiu, X., Audet, J., Wong, G., Pillet, S., Bello, A., Cabral, T., Strong, J.E., Plummer, F., Corbett, C.R., Alimonti, J.B., and Kobinger, G.P. (2012a). Successful treatment of ebola virus-infected cynomolgus macaques with monoclonal antibodies. Sci. Transl. Med. *4*, 138ra81.

Qiu, X., Fernando, L., Melito, P.L., Audet, J., Feldmann, H., Kobinger, G., Alimonti, J.B., and Jones, S.M. (2012b). Ebola GP-specific monoclonal antibodies protect mice and guinea pigs from lethal Ebola virus infection. PLoS Negl. Trop. Dis. *6*, e1575.

Qiu, X., Audet, J., Wong, G., Fernando, L., Bello, A., Pillet, S., Alimonti, J.B., and Kobinger, G.P. (2013a). Sustained protection against Ebola virus infection following treatment of infected nonhuman primates with ZMAb. Sci. Rep. *3*, 3365.

Qiu, X., Wong, G., Fernando, L., Audet, J., Bello, A., Strong, J., Alimonti, J.B., and Kobinger, G.P. (2013b). mAbs and Ad-vectored IFN-α therapy rescue Ebola-infected nonhuman primates when administered after the detection of viremia and symptoms. Sci. Transl. Med. *5*, 207ra143.

Qiu, X., Wong, G., Fernando, L., Ennis, J., Turner, J.D., Alimonti, J.B., Yao, X., and Kobinger, G.P. (2013c). Monoclonal antibodies combined with adenovirus-vectored interferon significantly extend the treatment window in Ebola virus-infected guinea pigs. J. Virol. *87*, 7754–7757.

Qiu, X., Wong, G., Audet, J., Bello, A., Fernando, L., Alimonti, J.B., Fausther-Bovendo, H., Wei, H., Aviles, J., Hiatt, E., et al. (2014). Reversion of advanced Ebola virus disease in nonhuman primates with ZMapp. Nature *514*, 47–53.

Scheres, S.H. (2012). RELION: implementation of a Bayesian approach to cryo-EM structure determination. J. Struct. Biol. *180*, 519–530.

Sorzano, C.O., Marabini, R., Velázquez-Muriel, J., Bilbao-Castro, J.R., Scheres, S.H., Carazo, J.M., and Pascual-Montano, A. (2004). XMIPP: a new generation of an open-source image processing package for electron microscopy. J. Struct. Biol. *148*, 194–204.

Suloway, C., Pulokas, J., Fellmann, D., Cheng, A., Guerra, F., Quispe, J., Stagg, S., Potter, C.S., and Carragher, B. (2005). Automated molecular microscopy: the new Leginon system. J. Struct. Biol. *151*, 41–60.

van Duijl-Richter, M.K., Hoornweg, T.E., Rodenhuis-Zybert, I.A., and Smit, J.M. (2015). Early events in Chikungunya virus infection-from virus cell binding to membrane fusion. Viruses *7*, 3647–3674.

Volchkov, V.E., Feldmann, H., Volchkova, V.A., and Klenk, H.D. (1998). Processing of the Ebola virus glycoprotein by the proprotein convertase furin. Proc. Natl. Acad. Sci. USA *95*, 5762–5767.

Volchkov, V.E., Chepurnov, A.A., Volchkova, V.A., Ternovoj, V.A., and Klenk, H.D. (2000). Molecular characterization of guinea pig-adapted variants of Ebola virus. Virology *277*, 147–155.

Voss, N.R., Yoshioka, C.K., Radermacher, M., Potter, C.S., and Carragher, B. (2009). DoG Picker and TiltPicker: software tools to facilitate particle selection in single particle electron microscopy. J. Struct. Biol. *166*, 205–213.

Wang, H., Shi, Y., Song, J., Qi, J., Lu, G., Yan, J., and Gao, G.F. (2016). Ebola viral glycoprotein bound to its endosomal receptor Niemann-Pick C1. Cell *164*, 258–268.

Whitt, M.A. (2010). Generation of VSV pseudotypes using recombinant ΔG-VSV for studies on virus entry, identification of entry inhibitors, and immune responses to vaccines. J. Virol. Methods *169*, 365–374.

Wong, A.C., Sandesara, R.G., Mulherkar, N., Whelan, S.P., and Chandran, K. (2010). A forward genetic strategy reveals destabilizing mutations in the Ebolavirus glycoprotein that alter its protease dependence during cell entry. J. Virol. *84*, 163–175.

Wong, G., He, S., Wei, H., Kroeker, A., Audet, J., Leung, A., Cutts, T., Graham, J., Kobasa, D., Embury-Hyatt, C., et al. (2015). Development and characterization of a guinea pig-adapted Sudan virus. J. Virol. *90*, 392–399.